Push-Pull Configuration of High Power MOSFETs for Generation of Nanosecond Pulses for Electropermeabilization of Isolated Cancer Stem Cells.

I. W. Davies[1,2], C. Merla[3], M. Tanori[3], A. Zambotti[4], J. Bishop[2], C. Palego[1] and C. P. Hancock[1,2]

[1]School of Electronic Engineering, University of Bangor, Bangor, United Kingdom.

[2]Creo Medical, Bath, United Kingdom.

[3]Division of Health Protection Technologies, ENEA-Casaccia, Rome 00123, Italy.

[4]Division of Resource Efficiency, ENEA-Casaccia, Rome 00123, Italy

***Abstract* — This paper presents the instrumentation and use of a novel electroporation generator, configured of MOSFETs in a push-pull configuration, with an artificial 50 Ω buffer for possible real-time neutralization of cancer stem cells. The results from an initial bench study investigates the development of an electroporation generator capable of delivering non-thermal treatment with an original cuvette housing unit and its effects on isolated cancer stem cell. Initial permeabilization investigation of cancer stem cells were conducted, indicating that the developed protocols and devices have a strong potential future use in achieving electro-manipulation of cancer stem cells.**

***Keywords* — electroporation, electro-manipulation, pulsed electric field, cancer stem cells, nanosecond pulses, high-voltage, push-pull, high power MOSFETs.**

I. Introduction

As part of European Union's Horizon 2020 research and innovation program, the SUMCASTEC project explores a new approach for real time isolation and neutralization of Cancer Stem Cells (CSCs), as Glioblastoma Multiforme (GBM) and Medulloblastoma (MB) via a novel micro-optofluidic lab-on-chip (LOC) platform [1]. An element of the deliverables is to develop an off-chip pulsed electric-field (EF), Electroporation (EP) or Irreversible Electroporation (IEP) generator [1]. GBM and MB are vicious primary brain tumours, occurring in adults and children respectively. Brain cancer result in more death per person than any other cancer, with 11,000 people diagnosed with a brain tumour in the UK in 2014, with a median survival rate of ~15 months; 5-year survival rate of ~4% [2]-[3].

IEP is relatively novel physical technique of ablation that has been successfully performed intraoperatively, laparoscopically and percutaneously [4]-[8]. The technique uses precisely controlled electric pulsed fields of short duration and high-voltage (HV) to alter a cell's transmembrane potential. This results in permeabilizing the cell's plasma membrane and disturbing intercellular homeostasis. The resultant permeabilization of cell plasma membrane can be reversible or irreversible leading in this case to cell death [4]-[8].

The EF based neutralization of CSCs could be mediated by cell electropermeabilization, but CSCs differentiation in the absence of EP seems another interesting possibility. The EP pulse duration and repetition frequency are low enough to ensure that the energy delivery into the biological system is non-thermal. Non-thermal HV EP approach seems a preferred method for neutralizing CSCs. This method allows targeted neutralization without heating the CSCs above body temperature. The non-thermal approach predominantly spares normal extracellular matrix, nearby vessels and structures, while allowing tissue regrowth and preventing unwanted damage to the patient's brain tissue and matrix [4]-[8].

II. Instrumentation

One of SUMCSTEC's technical milestones was to deliver a generator capable of pulse amplitude in excess of 1 kV, with pulse widths of 100 ns. Its modular design is based on a push-pull switching of HV, fast switching metal oxide semiconductor field effect transistor (MOSFET)s that are directly driven by opto-isolators with suitable switching times.

The ability of the modular design to generate the required pulses is dependent upon the switching times and maximum drain-source voltage of the MOSFETs. For this application it was important to choose a power MOSFET with a maximum drain-source voltage > 1 kV and total switching times (rise time (t_r) and fall time (t_f)) less than 100 ns (the actual values are: t_r = 10 ns and t_f = 60 ns). An n-channel enhancement type MOSFET device was used, where a positive gate-source voltage (V_{gs}) opens up the channel to control the drain current (i_D). The transconductance characteristic (i_D as a function of V_{gs}) was also considered carefully when choosing the most appropriate MOSFET to use. The selected opto-couplers operates as a gate driver, that requires to provides the necessary current to charge the gate-source and gate-drain capacitance (1), where C_{gate} is the gate capacitance [9]-[10].

Fig. 1 illustrates that an increase of gate voltage from 15 V to 20 V results in increased pulse amplitude experienced across a load. It also demonstrates that the developed EP generator performance exceeds the LTSpice simulation results across a purely 50 Ω resistor load. LTSpice model of the MOSFETs components where used for accurate simulation properties.

As discussed above, the power MOSFET was chosen by the fastest switching times (t_r and t_f), which in turn are determined by the time it takes to charge and discharge the gate-source and gate-drain capacitances (C_{total} (C_{in}) = (C_{gs} +

$C_{gd}(1+g_mR_L)$), where gm is the transconductance (i_D/V_{gs}) for the MOSFET of choice and RL the load impedance, which in this system varied from 10Ω to 60Ω. It is also chosen by the maximum drain-source voltage it's capable of handling before the device breaks down, i.e. $V_{D\text{-}S\ max}$ [9]-[10]. The gate driver or the opto-coupler chosen must provide enough current to charge/discharge the gate-source and gate-drain capacitances. It was found that by increasing the gate voltage by 5 V results in a 400 V increase in the pulse amplitude at the load (Fig. 1), as the current to charge the gate-source and gate-drain capacitance has increased. It can be said that gate voltage and gate current is proportional as capacitance of the MOSFET is constant in (1) ($i \propto V$). Fig. 1 simulation and measured result reinforce this theory [9]-[10].

$$i_D = C_{gate}\frac{dV_{gs}}{dt} \quad (1)$$

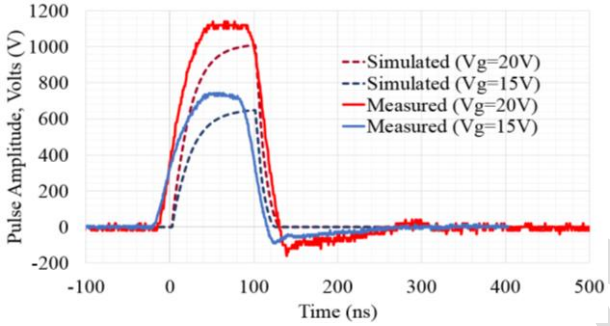

Fig. 1. Measured vs Simulated results on a 50 Ω resistor load.

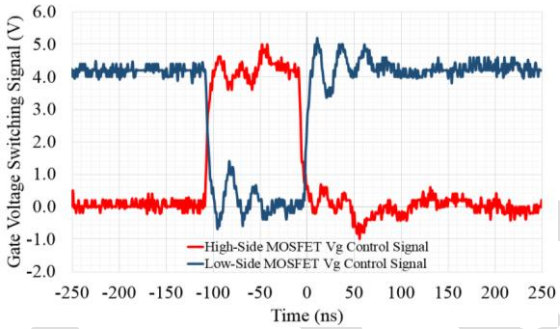

Fig. 2. Complimentary control signal of gate voltage for the high and low side push-pull MOSFET configuration for 100ns pulse.

The push-pull configuration of two MOSFETs switching topology means that the high-side MOSFET is 'off' most of the time while the low-side MOSFET is 'on'. The relationship between the two MOSFET switches is complimentary (Fig. 2). A key advantage of the push-pull arrangement is that it allows the amplitude of the voltage across the load (the peak pulse amplitude) to be twice the value that would be possible of a single ended arrangement was used. In the arrangement used in this work, the high-side MOSFET is 'on' and the low-sided MOSFET is 'off' when the nanosecond pulses are generated. The modular design is advantageous as a low-impedance path to ground is formed. This results faster fall-time as the low impedance path allows the HV signal to be discharge via the low-side MOSFET than the coaxial line and load to ground.

In addition to producing 1 kV, 100 ns pulses, the EP generator control and programming allow for a wide range of pulse profiles to be generated (Table 1). Fig. 3 indicates that the pulse amplitude is unaffected throughout its operating repetition frequencies (1-50 Hz). Furthermore, it suggests that the SPG performance is optimized in the pulse width range of 100 ns to 300 ns, for pulse amplitudes in excess of 1 kV.

Table 1. SPG performance characteristics

Parameters	Range	Comment
Frequency	1Hz-50Hz	Pulse repetition frequency
Pulse Width	80ns-1000ns	Increments of 10ns (between 80ns-400ns) and 20ns (between 400ns-1us)
Burst	1-1000	Number of pulses generated successively

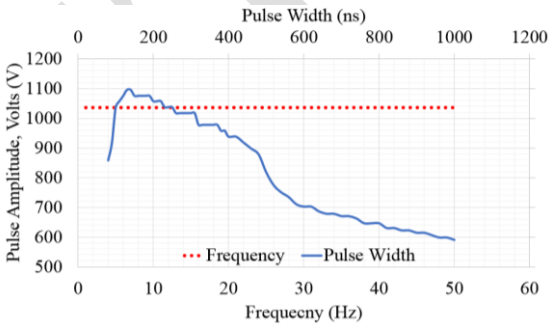

Fig. 3. SPG measured performance characteristic. How the pulse voltage amplitude generated at various operating frequency (at 100 ns pulse width) and pulse width (at 50 Hz).

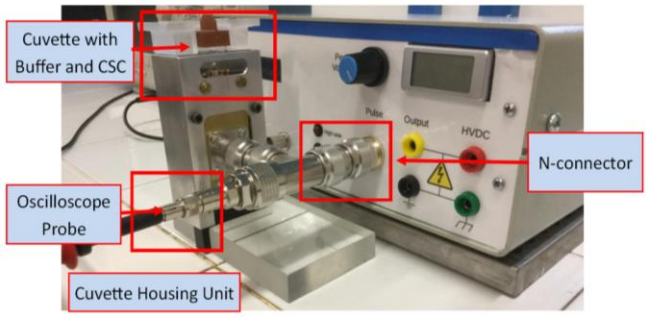

Fig. 4. Cuvette housing unit and SPG experiment set-up.

Exposing the CSCs to HV, 100 ns - 300 ns pulses were delivered via a cuvette housing unit designed by ENEA. This unit allows Bio-rads commercially available 0.1cm gap, 100µL EP cuvettes (1mm x 55mm^2), with the CSCs suspended in a specific 50Ω buffer (phosphate buffer saline and distilled water in a suitable dilution [10]), to be exposed to pulsed EF. The housing unit allows an easy connection with the generator (standard N-connector) with the possibility of pulse monitoring on an oscilloscope during pulse delivery. An optimized transition between the coaxial connector and the planar electrode of the EP cuvette was realized (Fig. 4). An artificial 50Ω buffer, of 0.3S/m conductivity, to suspend the CSCs was initially used to optimize impedance matching between the SPG and the CSCs load. The buffer consists of 20mL of phosphate saline buffer, 80mL of distilled water and

8.2g of sucrose [11]. The sucrose counteracts the occurrence of osmosis.

Prior to the CSCs exposure to pulse EF from SPG, YOPRO-1 dye (3µM) was added to the CSCs solution. If EP of the CSCs was successful, nanometer-sized pores in the cell's membrane would be created. The permeabilization of cells membranes allows the dye to enter the CSCs cytoplasm and bind with nucleic acids (DNA, RNA), thus the permeabilized CSCs will become fluorescent. YOPRO-1 emission at 510nm has been detected using florescence microscopy. The percentage of cell population that becomes florescent indicates the success of EP on the CSCs. The complete protocol for CSCs preparation can be followed here [11].

III. Result and Analysis

The previously mentioned artificial buffer was prepared to represent a 50 Ω load to aid impedance matching between the load and the generator. Fig. 5 suggests that the buffer load is 50 Ω, as the waveform measured with the buffer is comparable to the waveform measured with a 50 Ω resistor. Fig. 5 depicts the 100 ns, 200 ns and 300 ns pulse waveforms that were measured across the EP cuvette containing CSCs suspended with the 50 Ω, 0.3 S/m solution. These waveforms, shown in Fig. 5, illustrate the pulsed EF, per pulse, delivered to the CSCs during the primary permeabilization rate investigation. Table 2 illustrates the selected performance characteristic of SPG (pulse width, frequency, number of pulses) which resulted in various permeabilization rate of the populated CSCs within the sample.

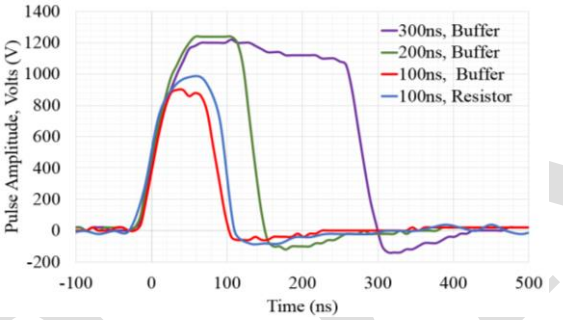

Fig. 5. 100 ns, 50 Hz, 20 burst waveform with 50 Ω resistor for SPG load (blue). And 100 ns (red), 150ns (green) and 300 ns (purple) pulse, 50 Hz, 20 bursts waveform measured with CSCs in the 50 Ω buffer load.

Table 2. indicates that exposing CSCs to 200 ns and 300 ns with 5 or more consecutive pulses results in >70% of the CSCs becoming permeabilized (green fluorescence in Fig. 6). Fig. 6. indicates that 90% of the CSCs population is fluorescent and permeabilized when 20 consecutive 1.2 kV pulses, of 300 ns duration are delivered though the cuvette.

A principle of EP is its non-thermal effect on the living organism. Table 3. demonstrates the heating effect of the EF applied on the CSCs buffer load with various SPG parameters. Equation (2) can be used to calculate the heating effect or the change in temperature the biological load experiences. It highlights that the EP effect was non-thermal, with an increase of 0.1x10-3 0C (100 µ0C) in the 100mL buffer temperature [12]. In (2), V is pulse amplitude (*Volts, V*), Z is load resistance (*50*Ω), P_w is pulse width (*seconds, s*) and D is duty cycle (*ratio*). E is energy (*Jules, J*), C is heat coefficient (*4.18 J/g/^{0}C as buffer consists mainly of water*), L indicating volume of biological load (*in millilitres*) and ΔT is the temperature change the biological load experiences (*degree Celsius, ^{0}C).*

Table 2. CSCs permeabilization rate following EP exposure by SPG

Pulse Width (ns)	E-field Strength (MV/m)	# of Pulses	Frequency (Hz)	Permeabilization Rate (%)
100	~0.9	1	50	0
100	~0.9	5	50	30
100	~0.9	10	50	27
100	~0.9	20	50	35
100	~0.9	20	1	5
200	~1.2	1	50	4
200	~1.2	5	50	74
200	~1.2	10	50	80
200	~1.2	20	50	83
200	~1.2	20	1	73
300	~1.2	1	50	18
300	~1.2	5	50	80
300	~1.2	10	50	81
300	~1.2	20	50	80
300	~1.2	20	1	90
Control	0	0	0	8

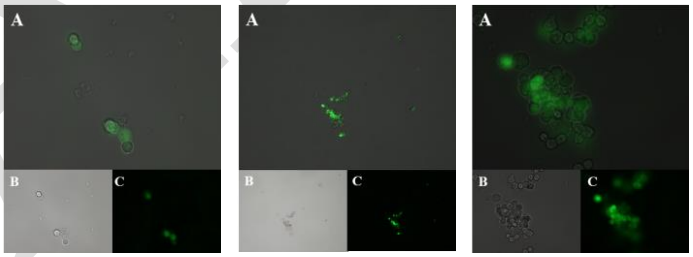

Fig. 6. Three different examples of permeabilized CSCs within a sample after exposure to 300 ns, ~1.2 MV/m, 20 pulses, 1Hz = 90%. A. bright field (visible light) superimposed on fluorescence microscope image, B. bright field (visible light) images. C. fluorescence microscope image.

$$\Delta T = \frac{(\frac{V^2}{Z}).P_w.D}{C.L} \quad (2)$$

Table 3. Heating of the CSCs/buffer

PW(ns)	V(kV)	R (Ω)	P(kW)	*f* (HZ)	E (mJ)	ΔT(µ^{0}C)
100	1.0	50	20.0	1	2.00	4.8
100	1.0	50	20.0	50	100.00	239.2
200	1.2	50	28.8	1	5.76	13.8
200	1.2	50	28.8	50	288.00	689.0
300	1.2	50	28.8	1	8.64	20.7
300	1.2	50	28.8	50	432.00	1033.0

Table. 3 highlights that the EP effect was non-thermal with a maximum increase of 0.1x10^{-3} ^{0}C (1000 µ^{0}C) the buffer experience with pulse properties of: 300 ns pulse width, 1.2 kV pulse amplitude, 50 continuous pulses. The result and mathematical theory indicate that the pulse properties effect

the biological load temperature. The heat coefficient, C and the volume, L in (2) is continuous, and therefore the change in the biological load temperature is dependent on the voltage amplitude, V, pulse width Pw and the duration the load is exposed to the pulses. ($\Delta T \propto D \propto P_w$). Wider the pulse width and the higher the magnitude of the pulse amplitude the more heating the load is exposed to and higher the temperature change the load experiences.

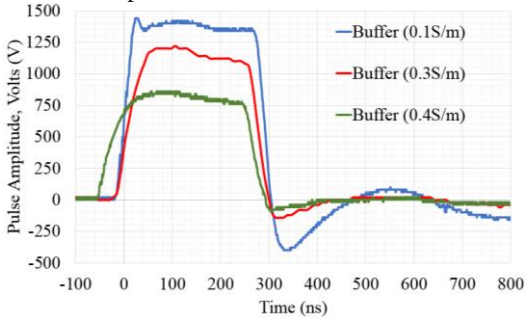

Fig. 7. 300 ns, 50 Hz, 20 burst pulse measured with various buffer solution at load. Solution conductivity of 0.1 S/m, 0.3 S/m and 0.4 S/m are reported.

Following initial investigation of exposing CSCs to controlled pulsed EF of short duration and HV, other buffer solutions of various conductivities where investigated (0.1 S/m, and 0.4 S/m) with pulse widths of 100 ns, 200 ns and 300 ns. Fig. 7 shows that the SPG performance is insensitive of the load impedance, in the range between 10 Ω (0.4 S/m) to 60 Ω (0.1 S/m), demonstrating broadband matching performance as far as the pulse waveform widths are considered. This effect shows good transition times preservation overall. However, the delivered pulse amplitude does change with the buffer impedance. Pulse Amplitude ($V_{amplitude}$) $\propto$ impedance at load (Z_{Load}). This effect is attributed to the low-impedance path of the switching topology adopted discussed in the instrumentation segment.

IV. Discussion and Conclusion

In conclusion, the overall system developed: the SPG, the cuvette housing unit, and the buffer resulted in successful permeabilization of the CSCs with the possibility of real-time pulse visualization via non-thermal EP. Promising results were obtained in terms of matching strategy and cell permeabilization to YOPRO-1 dye with various pulse durations. The gathered results do not reflect whether the CSCs are dead or alive after EP. Therefore, it is unknown whether they underwent reversible or irreversible EP. Additionally, it is important to state that this does not mean that the CSCs exposed to 100 ns pulses, which resulted in a lower fluorescent cell population, are not affected even if only poorly permeabilized. Viability studies are required to complement these preliminary experiments in the future. Further work will focus on the assessment of the optimized and suitable EF pulse parameters to maximally sensitize CSCs to standard oncological treatment, such as X-rays used in radiotherapy.

The generator developed is well matched to the application and has low sensitivity to various types of solution filling the cuvette. The low sensitivity and range of programmable pulse regimes in the SPG is advantageous to the user which performs well in comparison to more generic, commercial nanosecond generators such as *Schanffer NSG 504* HV pulse generator which is impedance sensitive.

The technique, within this initial bench study of using precisely controlled pulsed EF of short duration (nanoseconds) and HV, with the novel and versatile nanosecond pulse generator, alters a cell's transmembrane potential, and therefore permeabilize the CSC. In addition to this, the short duration of the pulses means a nonthermal HV EP approach is conducted. Possible utilization of this technique and HV EP generator, in vivo and vitro, could lead to a targeted neutralization without heating the CSCs and healthy normal extracellular matrix, nearby vessels and structures, above body temperature whilst simultaneously allowing tissue regrowth and preventing unwanted damage to the patient's brain tissue and matrix [4]-[8].

Acknowledgment

This project has received funding from the European Union's Horizon 2020 research and innovation program under grant agreement SUMCASTEC, No.737164. The authors would like to thank partners of the SUMCASTEC project for the successful collaboration and use of their facilities. We thank A. Casciati, M. Tanori, B. Tanno and M. Macuso from ENEA for the support in cell culturing and microscopy.

References

[1] "Home - SUMCASTEC", SUMCASTEC, 2018. [Online]. Available: http://www.sumcastec.eu/.

[2] "Tumor Types - National Brain Tumor Society", National Brain Tumor Society, 2018. [Online]. Available: http://braintumor.org/brain-tumor-information/understanding-brain-tumors/tumor-types/.

[3] Cancer Research UK, Cancerreasearchuk.org, 2018. [Online]. Available: http://www.cancerreasearchuk.org.

[4] R. Martin, K. McFarland, S. Ellis and V. Velanovich, "Irreversible Electroporation in Locally Advanced Pancreatic Cancer: Potential Improved Overall Survival", Annals of Surgical Oncology, vol. 20, no. 3, pp. 443-449, 2012.

[5] R. Martin, "Use of irreversible electroporation in unresectable pancreaticCancer", HepatoBiliary Surgery and Nutrition. Vol. 4, no. 3, pp. 221-215, 2015

[6] S. Bagla and D. Papadouris, "Percutaneous Irreversible Electroporation of Surgically Unresectable Pancreatic Cancer: A Case Report", J. of Vascular and Interventional Radiology, vol. 23, no. 1, pp. 142-145, 2012.

[7] N. Jourabchi, K. Beroukhim, B. Tafti, S. Kee and E. Lee, "Irreversible electroporation (NanoKnife) in cancer treatment", Gastrointestinal Intervention, vol. 3, no. 1, pp. 8-18, 2014.

[8] R. Sundararajan, Electroporation-based therapies for cancer. Waltham, MA: Woodhead Pub, 2014.

[9] C. Hancock, "Pulsed field systems for analysing the switching process in particulate recording media", Ph.D, Univeristy of Wales, Bangor, 1995.

[10] R. Severns, Siliconix poweer application handbook, Siliconix incorparated, Santa Clara, California, 1985.

[11] C. Merla, A. Casciati, M. Tanori, B. Tanno and M. Mancuso, "SUMCASTEC_180123_NA_protocolWP3_protocol_.pdf_Rome_C. Merla_Partners and public_NA", Zenodo, 2018. [Online]. Available: https://zenodo.org/record/1157784#.Wm9N3a5l-po.

[12] C. Merla, N. Ticaud, D. Arnaud-Cormos, B. Veyret and P. Leveque, "Real-Time RF Exposure Setup Based on a Multiple Electrode Array (MEA) for Electrophysiological Recording of Neuronal Networks", IEEE Trans. Microw. Theory Tech., vol. 59, no. 3, pp. 755-762, 2011.